Journal of the Franklin Institute 362 (2025) 107394

Contents lists available at ScienceDirect

Journal of the Franklin Institute

journal homepage: www.elsevier.com/locate/fi

Chattering-free and finite-time estimation of the time-varying geometrical center for the multi-targets enclosing control problem

Liang Zhang [a], Jun Song [b], Shuping He [a,*]

[a] School of Electrical Engineering and Automation, Anhui university, Hefei, 230601, China
[b] School of Artificial Intelligence, Anhui university, Hefei, 230601, China

ARTICLE INFO

Keywords:
Chattering free estimators
Finite-time stabilization
Multi-Robot System (MRS)
GCT
MTECP

ABSTRACT

This paper investigates the finite-time estimation of the time-varying Geometrical Center of Targets (GCT) in Multi-Target Enclosing Control Problem (MTECP). Existing estimators exhibit a chattering phenomenon that is harmful to the mechanical components of the deployed robots when forming the enclosing formation. We thereby propose two chattering-free finite-time estimators, employing a fully distributed approach demanding only the local observation and neighboring communication. The first fractional-order estimator is formulated by replacing the discontinuous term in the existing finite-time estimator by a fractional-order term, which remains smooth when the consensus error approaches zero. Theoretical results show that the estimation error can be stabilized into a bounded region adjustable by tuning the parameters. Then, another novel estimator with double integral architecture is designed to further eliminate the bounded estimation error in the first-order estimator i.e. can achieve exact tracking of the GCT in finite-time. Its continuity of estimation arises from the integration of a discontinuous unit-vector term and three more internal states are introduced to realize the double integral architecture. Finally, simulation and comparison results validate the correctness and smoothness of the proposed estimators.

1. Introduction

The concept of enclosing formation has gained significant traction in natural swarms, particularly for its potential advantages in predation and protection, as evidenced in the works [1,2]. This heightened interest has spurred increased attention toward surrounding and enclosing control problems in recent years, typically, aimed at achieving a formation for a group of followers, enabling them to revolve around a common point while maintaining a predefined spacing pattern. The primary goal is to ensure that the formation can contain single or multiple targets at all times.

Most enclosing works concentrated on the single-target case due to its potential applications of attacking, entrapping, or protecting target objects. Results on the single-static-target enclosing problem are detailed in [3–5]. When the target is observable, these works formulate and solve the problem by creating an encircling formation centered on the target. However, enclosing a single moving target becomes more challenging due to varying observation topologies between mobile agents and the moving target. Assuming knowledge of the target's velocity, cyclic pursuit strategies were developed for holonomic agents in [6] and more general MIMO agents in [7]. Besides, [8] proposed a local information control law to enclosing the single moving target with bounded and unknown velocity. In relation to the diverse variants in this field, practical constraints on the observations and circular formation have been imposed in both obstacle-laden [9] and obstacle-free [10] environments. Moreover, the elliptical enclosing

* Corresponding author.
E-mail address: shuping.he@ahu.edu.cn (S. He).

https://doi.org/10.1016/j.jfranklin.2024.107394
Received 29 February 2024; Received in revised form 21 August 2024; Accepted 5 November 2024
Available online 14 November 2024

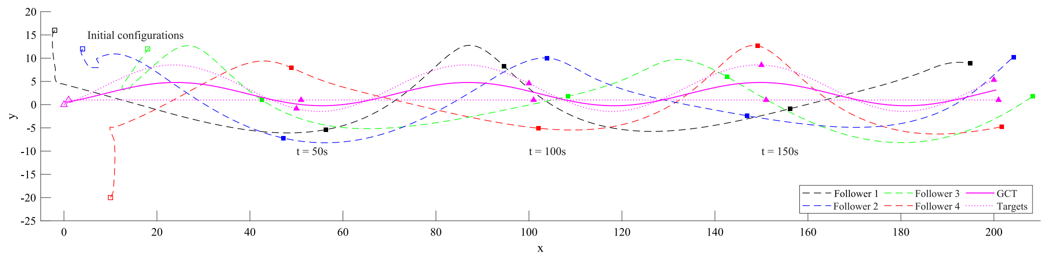

Fig. 1. Trajectory demonstration of the multi-moving-target enclosing problem using four followers and two targets.

control problem was considered in [11] where a finite-time composite learning-based enclosing controller was proposed. More recent works on the single-moving-target enclosing problem can be found on addressing linear dynamics with input saturation in [12,13], nonholonomic agents using feedback linearization in [14], mobile targets with time-varying velocity and collision avoidance in [15], under-actuated autonomous surface vehicles with an event-triggered control framework in [16] and limited measurements in critical environments [17], among others.

Comparatively, MTECP poses heightened challenges as agents are required to orbit around the geometrical center of all targets as shown in Fig. 1. The key difficulty is that this circular center remains imperceptible and unobservable to all followers. As a result, each follower must maintain a supplementary estimator to distributively approximate the position of this unobservable center, utilizing their individual observations and information exchanged with neighboring robots. An exponential estimator is proposed in [18,19] for both the first- and second-order MRS to form a convex hull containing multiple static targets. Then an average-consensus-based estimator [20] is introduced into the enclosing problem of multiple moving targets in [21,22]. Besides, the centralized-form least-square (LS) estimator is presented in [23] using bearing-only measurements to localize each target and estimate the geometric center. However, all the estimators mentioned above are exponentially stable. The impact on control stability of the accumulated tracking error between the estimated position and the real GCT have not been thoroughly investigated. The accumulated error may lead to fatal divergence during the enclosing stage in some critical environments, prompting the development of a finite-time convergent estimator in [24–27]. This finite-time convergent estimator guarantees precise tracking of the target geometric center (TGC) within a finite time frame, ensuring that the accumulated error during the enclosing stage remains within tolerable limits.

However,current finite-time estimator still exhibits the chattering phenomenon caused by the discontinuous term (see Figure 3 in [24]) when the estimator is getting convergent, or the estimator's output of adjacent agents becomes similar. Chattering in robot systems manifests as rapid and erratic oscillations in signals, leading to instability in robot movements. This instability can compromise the robot's ability to execute tasks with precision and accuracy, and in the worst-case scenario can result in increased wear and tear on the mechanical components. As the controller of the MTECP composites the encircling and mincing motion, the output of estimator is directly feed-forward to the controller. Therefore, the chattering estimations in [24–28] degrade the control performance and are harmful to the actuator. While a smoothing function is suggested in [24] to address this issue, further evidence is needed to substantiate the efficacy of finite-time convergence, and the impact on the accuracy of the enclosing formation warrants additional investigation.

Regarding the aforementioned issues, this paper addresses the problem of continuously distributed estimation of the time-varying GCT in finite-time within the context of the MTECP. Two chattering-free estimators are designed, with one utilizing the consensus error with fractional order, while the other employs double integration to ensure continuity. The innovations are highlighted as follows:

- Contrasting to most existing single-target cases in [9–16,29], the enclosing problem considered in this work is the multi-moving-target case, which is more challenging as the circular center of enclosing formation is unperceptive. Hence the finite-time and distributed estimation for the GCT is critical. This work investigates the finite-time and distributed estimation of the GCT for MTECP capable of multi-moving-target cases.
- Different from the multi-target enclosing problem in [24–27], this work focuses on removing the chattering phenomenon for the finite-time estimation of the time-varying GCT that is harmful to the mechanical components of the robots. Therefore, the lifespan of actuators can be extended using the proposed methods.

The rest of this work is organized as follows. The notations and some important lemmas are first introduced in Section 2. Then the problem of enclosing control for multiple moving targets is formulated and the impact of the chattering phenomenon on the MTECP is analyzed in Section 3. It follows with the main results of this work, the two proposed estimators and their derivations to show the finite-time stability and continuity in Section 4. Finally, the simulation and conclusion are presented at the end of this work.

2. Preliminaries

Notations. In this work, we use the normal lowercase to represent the scalar i.e. $x \in \mathscr{R}^1$ and bold for the vector i.e. $\boldsymbol{x} \in \mathbb{R}^n, n \geq 2$ respectively. The operator $|\cdot|$ denotes the absolute value of a scalar or the number of elements of a vector. Without any specification, $\|\cdot\|$ denotes the Euclidean norm of the inputted vector.

At first, the following result [30] is provided to guarantee the finite-time stability,

Theorem 1. *Consider the nonlinear system $\dot{\boldsymbol{x}} = f(\boldsymbol{x})$ with $f(\mathbf{0}) = \mathbf{0}$, suppose that there exist a C^1 positive function $V(\boldsymbol{x}_0)$ and two real numbers $c > 0, \alpha \in (0,1)$, such that the inequality*

$$\dot{V}(\boldsymbol{x}) \le -cV^{\alpha}(\boldsymbol{x})$$

holds, then the system is finite-time stable and the upper bound of the settling time is given by

$$T \le \frac{V^{1-\alpha}(\mathbf{0})}{c(1-\alpha)}$$

Additionally, for any real constant $\gamma < V(\mathbf{0})$, then the settling time T_1 that ensures $V(t) < \gamma, \forall t > T_1$ can be bounded by

$$T_1 \le \frac{V^{1-\alpha}(\mathbf{0}) - \gamma^{1-\alpha}}{c(1-\alpha)}.$$

Next, the following two lemmas are instrumental in simplifying the derivations of our main results,

Lemma 1. *Given a vector $\boldsymbol{x} \in \mathbb{R}^n$ and a positive $0 < p < 1$, then we have $\left(\sum_{i=1}^n |x_i|\right)^p \le \sum_{i=1}^n |x_i|^p \le n^{1-p}\left(\sum_{i=1}^n |x_i|\right)^p$*

Lemma 2. *Given two sets of functions $\{b_1(t), b_2(t), \dots, b_n(t)\}$, $\{c_1(t), c_2(t), \dots, c_n(t)\}$ and a symmetric matrix $\boldsymbol{A} = [a_{ij}] \in \mathbb{R}^{n\times n}$, then*

$$\sum_{i=1}^{n}\sum_{j=1}^{n}\left[a_{ij}c_i(t)\left[b_i(t) - b_j(t)\right]^{\frac{q}{p}}\right] = \frac{1}{2}\sum_{i=1}^{n}\sum_{j=1}^{n}\left\{a_{ij}\left[c_i(t) - c_j(t)\right]\left[b_i(t) - b_j(t)\right]^{\frac{q}{p}}\right\}$$

where $p, q > 0$ are two odd positives. In addition, if $c_i(t) = b_i(t), \forall i \in \{1,2,\dots,n\}$, then

$$\sum_{i=1}^{n}\sum_{j=1}^{n}\left[a_{ij}c_i(t)\left[b_i(t) - b_j(t)\right]^{\frac{q}{p}}\right] = \frac{1}{2}\sum_{i=1}^{n}\sum_{j=1}^{n}\left\{a_{ij}\left[b_i(t) - b_j(t)\right]^{1+\frac{q}{p}}\right\}$$

And especially when $c_i(t) = 1, \forall i \in \{1,2,\dots,n\}$,

$$\sum_{i=1}^{n}\sum_{j=1}^{n}\left[a_{ij}\left[b_i(t) - b_j(t)\right]^{\frac{q}{p}}\right] = 0$$

3. Problem formulation

3.1. Mathematics formulation of the MTECP

Consider a group of n agents, called the followers, are deployed in a 2-D plane, with the first-order integrator system as:

$$\dot{\boldsymbol{p}}_i = \boldsymbol{u}_i, \forall i \in \mathscr{V}_F = \{1,2,\dots,n\} \tag{1}$$

Their mission is to encircle around a group of m targets $j \in \mathscr{V}_L = \{1,2,\dots,m\}$ with a predefined spacing pattern. Note that the targets may be uncooperative and therefore their dynamics are also unknown in practice. Here we represent the targets using a second-order equation as follows:

$$\begin{cases} \dot{\boldsymbol{p}}_j^t = \boldsymbol{v}_j^t \\ \dot{\boldsymbol{v}}_j^t = \boldsymbol{a}_j^t \end{cases}, \forall j \in \mathscr{V}_L \tag{2}$$

where $\boldsymbol{p}_j^t, \boldsymbol{v}_j^t, \boldsymbol{a}_j^t \in \mathbb{R}^2$ are the position, velocity and acceleration of the jth target respectively and $\boldsymbol{a}_j^t$ is unknown . $\boldsymbol{p}_i, \boldsymbol{u}_i$ are the position and control input of the ith follower. As demonstrated in Fig. 2, the GCT can be defined as

$$\bar{\boldsymbol{p}}^t = \frac{1}{m}\sum_{i\in\mathscr{V}_L}\boldsymbol{p}_i^t \tag{3}$$

Then the concept of the included angle is important for further description of the enclosing problem, whose definition is given as,

$$\begin{aligned} \bar{\theta}_i &= \theta_{i_+} - \theta_i + \varsigma_i \\ \varsigma_i &= \begin{cases} 0, & \text{if } \theta_{i_+} - \theta_i \ge 0 \\ 2\pi, & \text{if } \theta_{i_+} - \theta_i < 0 \end{cases} \end{aligned} \tag{4}$$

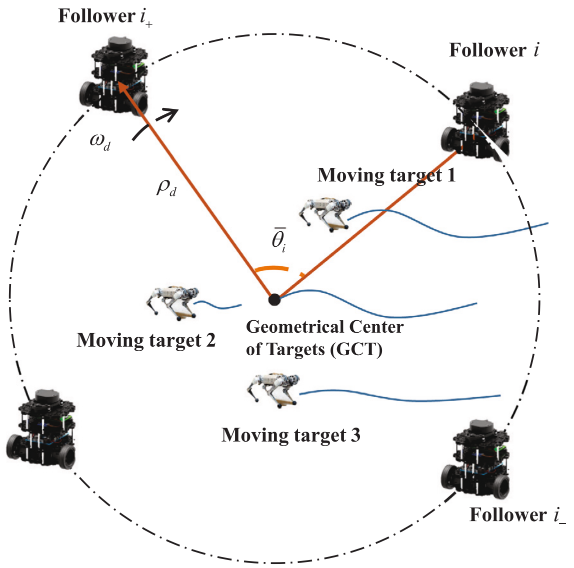

Fig. 2. Configuration for the enclosing problem, where i_+, i_- denote the successor and predecessor of the follower i according to the neighboring strategy in [8,15], ρ_d, ω_d are the expected enclosing radius and rotating angular velocity respectively, $\bar{\theta}_i$ is the included angle between the follower i and its successor i_+.

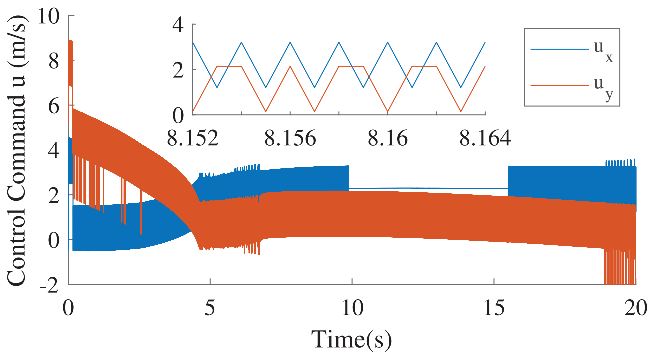

Fig. 3. Control commands of the first follower during the enclosing process shown in Fig. 1 using the finite-time GCT estimator (5) and finite-time controller (6).

where $\theta_i = atan2(\frac{\Delta p_i^y}{\Delta p_i^x})$ is the relative angle between the follower i and the GCT in the global frame. $\Delta p_i^x, \Delta p_i^y$ are the elements in the relative position vector $\boldsymbol{\Delta p}_i$ between follower i and the GCT i.e. $\boldsymbol{\Delta p}_i = \boldsymbol{p}_i - \bar{\boldsymbol{p}}^t$.

The objective of the MTECP is to design a proper distributed control law $\boldsymbol{u}_i$ such that these targets can be surrounded by a convex hull spanned by all followers. The common enclosing formation is a circle encoded by $\mathscr{P} = \{w_d, \rho_d, \bar{\boldsymbol{\theta}}_d\}$ centered at the GCT with a predefined radius $\rho_d > max_{i\in \mathscr{V}_L}(\|\boldsymbol{p}_i^t - \bar{\boldsymbol{p}}^t\|)$ and rotating angular speed $\omega_d > 0$. Additional tasks also specify a spacing pattern indicated by a set of included angles $\bar{\boldsymbol{\theta}}_d = [\bar{\theta}_{1d}, \bar{\theta}_{2d}, \dots, \bar{\theta}_{nd}]^T\, s.t. \sum_{i=1}^n \bar{\theta}_{id} = 2\pi$.

Graph Theory: The interaction in MTECP can be categorized into the communication among followers and the observation between followers and targets. We assume the **communication topology** to be an undirected graph $\mathscr{G}_1 = \{\mathscr{V}_F, \mathscr{E}_F, \boldsymbol{A}\}$ consisting of n followers serving as the node set and $\mathscr{E}_F = \{(i,j) \in \mathscr{V}_F \times \mathscr{V}_F\}$ denoting the edge set. The ith and jth followers are said to be adjacent if $(i,j) \in \mathscr{E}_F$. The adjacent matrix $\boldsymbol{A} = [a_{ij}]$ is defined by $a_{ij} = a_{ji} = 1$ if $(i,j) \in \mathscr{E}_F$, otherwise $a_{ij} = 0$. The Laplacian matrix is defined as $\boldsymbol{L} = \boldsymbol{D} - \boldsymbol{A}$ where $\boldsymbol{D} = diag[d_1, d_2, \dots, d_n]$ with $d_i = \sum_{j=1}^n a_{ij}$. If the graph $\mathscr{G}_1$ is connected i.e. every two nodes in the graph can find a sequence of edges connecting them, the eigenvalues of the Laplacian matrix $\boldsymbol{L}$ is $0 = \lambda_1 \le \lambda_2 \le \cdots \le \lambda_n$. The **observation topology** is a unidirectional graph $\mathscr{G}_2 = \{\mathscr{V}_F, \mathscr{V}_L \mathscr{E}_{obs}, \boldsymbol{B}\}$ starting from the set of followers $\mathscr{V}_F$ to the targets $\mathscr{V}_L$. Similarly, the edge set is $\mathscr{E}_{obs} = \{(i,j) \in \mathscr{V}_F \times \mathscr{V}_L\}$ and the observation matrix $\boldsymbol{B} = [b_{ij}]$ is defined by $b_{ij} = 1$ if $i \in \mathscr{V}_F, j \in \mathscr{V}_L, (i,j) \in \mathscr{E}_{obs}$. We denote three neighboring sets $\boldsymbol{N}_i^t = \{\forall j | j \in \mathscr{V}_L, (i,j) \in \mathscr{E}_{obs}\}$ containing the targets that ith follower can observe, $\boldsymbol{N}_j^F = \{\forall i | i \in \mathscr{V}_i, (i,j) \in \mathscr{E}_{obs}\}$

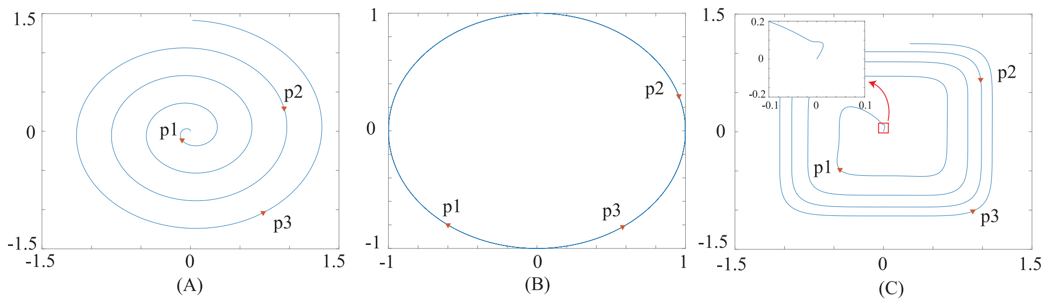

Fig. 4. (A): the evolution of the vector $\boldsymbol{p} \in \mathbb{R}^2$ along a spiral line; (B): the discontinuous transformation of $\boldsymbol{p}/\|\boldsymbol{p}\|$ as a circle of unit vector and (C): the fractional-order transformation of $\boldsymbol{p}^{\frac{1}{3}}$.

including the followers that can observe the jth targets and $\boldsymbol{N}_i = \{\forall j | j \in \mathscr{V}_F, (i, j) \in \mathscr{E}_F\}$ the set of followers that ith follower can communicate with.

3.2. Chattering problem of estimating the GCT in finite-time

How to acquire the GCT is one of the key issues in the multi-target enclosing problem. The most intuitive method is to calculate according to its definition in (3) by assuming at least one follower can observe all targets all the time and then communicate this information with other connected followers. If the communication network among followers is connected, the GCT can be delivered to all followers quickly using a multi-hop routing method. However, such an assumption is too strong to be applied in reality because most followers can only observe part of targets due to various observation limitations.

In this regard, existing works tend to decouple the enclosing problem for multi-moving-target cases into two phases:

Phase I: Designing a finite-time estimator for the position and velocity of GCT using only local information, for example, the observations of a subset of neighboring targets and the exchanged messages from other adjacent followers. e.g.

$$\begin{cases} \boldsymbol{r}_i = \boldsymbol{\Phi}_i + \tilde{\boldsymbol{p}}_i, \qquad \tilde{\boldsymbol{p}}_i = \dfrac{n}{m} \displaystyle\sum_{j \in \boldsymbol{N}_i^T} \dfrac{1}{|\boldsymbol{N}_j^F|} \boldsymbol{p}_j^t \\ \dot{\boldsymbol{\Phi}}_i = k_{sgn} \displaystyle\sum_{j \in \boldsymbol{N}_i} \dfrac{\boldsymbol{r}_j - \boldsymbol{r}_i}{\|\boldsymbol{r}_j - \boldsymbol{r}_i\|} \end{cases} \tag{5}$$

which has been well-studied in [24–27]. Results show that the output of this estimator $\boldsymbol{r}_i$ can exactly track the real GCT in finite time under some mild assumptions.

Phase II: Proposing a formation controller by directly feedforward the estimates to track the movements of all targets after the convergence of the finite-time estimator. For example, a finite-time controller for encircling formation with arbitrary space pattern is designed in our previous work [31]:

$$\begin{cases} \boldsymbol{u}_i = \boldsymbol{\varphi}_i^T w_{z,i} + \boldsymbol{\varphi}_{i,\perp}^T w_{\delta,i} + \dot{\boldsymbol{r}}_i \\ w_{z,i} = -k_z z_i^{\frac{1}{\alpha_0}} \\ w_{\delta,i} = k_\delta \delta_i^{\frac{1}{\alpha_0}} + w_d \end{cases} \tag{6}$$

where $\boldsymbol{\varphi}_i = [\cos(\theta_i), \sin(\theta_i)]^T$ is the unit vector of $\boldsymbol{\Delta p}_i$ and $\boldsymbol{\varphi}_{i,\perp}$ is the perpendicular vector of $\boldsymbol{\varphi}_i$ in the clockwise direction. $\dot{\boldsymbol{r}}_i$ is the derivative of the output of the finite-time estimator (5). z_i, δ_i are the radius error and included angle error generated by $\mathscr{P}$ the expected formation and $\boldsymbol{r}$ the estimated counterpart of the GCT, α_0, k_z, k_δ are the parameters, and w_d is the desired rotating speed.

Remark 1. The discontinuity of the estimator (5) comes from the unit-vector term $\frac{\boldsymbol{r}_i - \boldsymbol{r}_j}{\|\boldsymbol{r}_i - \boldsymbol{r}_j\|}$ as demonstrated in Fig. 4(B). The unit-vector term remains on the circle until the consensus is achieved i.e. $\boldsymbol{r}_i = \boldsymbol{r}_j, \forall i, j$. Therefore, any small difference between two neighboring estimators will result in frequent changes in the direction of the unit vector, which is observed as chattering.

Remark 2. As shown in (6), the output of the estimator $\boldsymbol{r}_i$ and its derivative $\dot{\boldsymbol{r}}_i$ are directly used in the controller, on which the continuity of the controller depends. However, current finite-time estimator for multiple moving targets (5) contains the discontinuous term $\frac{\boldsymbol{r}_j - \boldsymbol{r}_i}{\|\boldsymbol{r}_j - \boldsymbol{r}_i\|}$, which results in chattering when either the estimator is getting convergent, or the estimates of two adjacent agents become similar. Since the estimates and the derivative of estimates will be directly feedforward to the controller in most prevailing methods, the discontinuity in the estimator will bring chattering to the control input of the follower, see Fig. 3, which is harmful to the actuators. Therefore, it is necessary to develop innovative estimators whose estimated position and velocity are both continuous.

The following assumptions regarding the communication and observation topology form the basis of our continuous estimators.

Assumption 1. The communication topology among followers is undirect and connected. The communication weights are either 0 or 1.

Assumption 2. Each leader can be observed by at least one follower during the enclosing.

Assumption 3. The velocity $\boldsymbol{v}_j$ and acceleration $\boldsymbol{a}_j$ of GCT are piece-wisely continuous and are bounded by the known positive constants β and γ such that

$$\|\boldsymbol{v}_j^t\| \le \beta, \|\boldsymbol{a}_j^t\| \le \gamma, \forall j \in \mathscr{V}_L$$

4. Continuous finite-time estimators

This section proposes two distributed and continuous estimators to compute the GCT on every follower. Section 4.1 presents a variant of the discontinuous one in (5) by using the fractional-order of the consensus error, which can allow the error to remain in the vicinity of zero and therefore reduce the chattering. Section 4.2 considers a second-order estimator by integrating the discontinuous term, by which the derivative of $\boldsymbol{r}_i$ can be smoothing and continuous.

4.1. The fractional-order continuous estimator

Regarding the chattering estimator (5), we change the discontinuous term by the fractional-order consensus error as follows,

$$\begin{cases} \boldsymbol{r}_i = \boldsymbol{\Phi}_i + \tilde{\boldsymbol{p}}_i, \qquad \tilde{\boldsymbol{p}}_i = \dfrac{n}{m} \displaystyle\sum_{j \in \boldsymbol{N}_i^T} \dfrac{1}{|\boldsymbol{N}_j^F|} \boldsymbol{p}_j \\ \dot{\boldsymbol{\Phi}}_i = k_e \displaystyle\sum_{j \in \boldsymbol{N}_i} a_{ij} \left(\boldsymbol{r}_j - \boldsymbol{r}_i\right)^{\frac{1}{\alpha_1}} \end{cases} \tag{7}$$

where $\alpha_1 = \frac{p_1}{q_1}$, and $p_1 > q_1 > 0$ are positive odds. $k_e > 0$ is the estimator gain. To show its effectiveness, the candidate Lyapunov function is chosen as:

$$V_1 = \frac{1}{2} \sum_{i,j=1}^{n} \|\boldsymbol{r}_i - \boldsymbol{r}_j\|^2 = \frac{1}{2} \sum_{i,j=1}^{n} \left(\boldsymbol{r}_i - \boldsymbol{r}_j\right)^T \left(\boldsymbol{r}_i - \boldsymbol{r}_j\right) \tag{8}$$

Taking the derivative of both sides yields

$$\begin{aligned} \dot{V}_1 &= \frac{1}{2} \sum_{i,j=1}^{n} \left[(\dot{\boldsymbol{r}}_i - \dot{\boldsymbol{r}}_j)^T \left(\boldsymbol{r}_i - \boldsymbol{r}_j\right) + \left(\boldsymbol{r}_i - \boldsymbol{r}_j\right)^T (\dot{\boldsymbol{r}}_i - \dot{\boldsymbol{r}}_j) \right] \\ &= \sum_{i,j=1}^{n} \left[\left(\boldsymbol{r}_i - \boldsymbol{r}_j\right)^T (\dot{\boldsymbol{\Phi}}_i - \dot{\boldsymbol{\Phi}}_j) + \left(\boldsymbol{r}_i - \boldsymbol{r}_j\right)^T (\dot{\tilde{\boldsymbol{p}}}_i - \dot{\tilde{\boldsymbol{p}}}_j) \right] \end{aligned} \tag{9}$$

Then let substitute the estimator in (7), we can get

$$\begin{aligned} \dot{V} &= \sum_{i,j=1}^{n} \left[-k_e \left(\boldsymbol{r}_i - \boldsymbol{r}_j\right)^T \sum_{s_1=1}^{n} a_{is_1} \left(\boldsymbol{r}_i - \boldsymbol{r}_{s_1}\right)^{\frac{1}{\alpha_1}} \right. \\ &\left. -k_e \left(\boldsymbol{r}_i - \boldsymbol{r}_j\right)^T \sum_{s_2=1}^{n} a_{js_2} \left(\boldsymbol{r}_{s_2} - \boldsymbol{r}_j\right)^{\frac{1}{\alpha_1}} + \left(\boldsymbol{r}_i - \boldsymbol{r}_j\right)^T (\dot{\tilde{\boldsymbol{p}}}_i - \dot{\tilde{\boldsymbol{p}}}_j) \right] \\ &= -\frac{k_e}{2} \sum_{i,j=1}^{n} \left(\sum_{s_1=1}^{n} a_{is_1} (\boldsymbol{r}_i - \boldsymbol{r}_{s_1})^{\frac{1+\alpha_1}{\alpha_1}} + \sum_{s_2=1}^{n} a_{js_2} (\boldsymbol{r}_j - \boldsymbol{r}_{s_2})^{\frac{1+\alpha_1}{\alpha_1}} \right) + \\ & k_e \sum_{i=1}^{n} \boldsymbol{r}_i \sum_{j,s_2=1}^{n} a_{js_2} (\boldsymbol{r}_j - \boldsymbol{r}_{s_2})^{\frac{1}{\alpha_1}} + k_e \sum_{j=1}^{n} \boldsymbol{r}_j \sum_{i,s_1=1}^{n} a_{is_1} (\boldsymbol{r}_i - \boldsymbol{r}_{s_1})^{\frac{1}{\alpha_1}} \\ &+ \sum_{i,j=1}^{n} \left[\left(\boldsymbol{r}_i - \boldsymbol{r}_j\right)^T (\dot{\tilde{\boldsymbol{p}}}_i - \dot{\tilde{\boldsymbol{p}}}_j) \right] \end{aligned} \tag{10}$$

Recalling Lemma 2 follows

$$\begin{aligned} &\sum_{j=1}^{n} \sum_{s_2=1}^{n} a_{js_2} (\boldsymbol{r}_j - \boldsymbol{r}_{s_2})^{\frac{1}{\alpha_1}} = 0 \\ &\sum_{i=1}^{n} \sum_{s_1=1}^{n} a_{is_1} (\boldsymbol{r}_i - \boldsymbol{r}_{s_1})^{\frac{1}{\alpha_1}} = 0 \end{aligned} \tag{11}$$

Therefore, we can rewrite the derivative as:

$$
\begin{aligned}
\dot{V}_1 &= -\frac{nk_e}{2}\left[\sum_{i,s_1=1}^{n} a_{is_1}\left(\boldsymbol{r}_i-\boldsymbol{r}_{s_1}\right)^{\frac{1+\alpha_1}{\alpha_1}} + \sum_{js_2=1}^{n} a_{js_2}\left(\boldsymbol{r}_j-\boldsymbol{r}_{s_2}\right)^{\frac{1+\alpha_1}{\alpha_1}}\right] \\
&\quad + \sum_{i,j=1}\left[\left(\boldsymbol{r}_i-\boldsymbol{r}_j\right)^T(\dot{\tilde{\boldsymbol{p}}}_i-\dot{\tilde{\boldsymbol{p}}}_j)\right] \\
&= -nk_e\sum_{i,s_1=1}^{n} a_{is_1}\left(\boldsymbol{r}_i-\boldsymbol{r}_{s_1}\right)^{1+\frac{1}{\alpha_1}} + \sum_{i,j=1}\left[\left(\boldsymbol{r}_i-\boldsymbol{r}_j\right)^T(\dot{\tilde{\boldsymbol{p}}}_i-\dot{\tilde{\boldsymbol{p}}}_j)\right] \\
&\le -nk_e\sum_{i,s_1=1}^{n} a_{is_1}\left(\boldsymbol{r}_i-\boldsymbol{r}_{s_1}\right)^{1+\frac{1}{\alpha_1}} + 2\sum_{i,j=1}\left[\|\dot{\tilde{\boldsymbol{p}}}_i\|^{\frac{1}{2}}\|\boldsymbol{r}_i-\boldsymbol{r}_j\|^2\right]
\end{aligned} \tag{12}
$$

From the definition of $\tilde{\boldsymbol{p}}_i$ and Assumption 2, we know that $|\boldsymbol{N}_j^F| \ge 1$ and $|\boldsymbol{N}_i^T| \le m$, which yields

$$
\begin{aligned}
\|\dot{\tilde{\boldsymbol{p}}}_i\| &\le \frac{n}{m}\sum_{j\in\boldsymbol{N}_i^T}\frac{1}{|\boldsymbol{N}_j^F|}\|\dot{\boldsymbol{p}}_j^t\| \\
&\le n\max_{j\in\mathcal{V}_T}\|\dot{\boldsymbol{p}}_j^t\| = n\beta
\end{aligned}
$$

As a result,

$$
\begin{aligned}
\dot{V}_1 &\le -nk_e\sum_{i,s_1=1}^{n} a_{is_1}\left(\boldsymbol{r}_i-\boldsymbol{r}_{s_1}\right)^{1+\frac{1}{\alpha_1}} + 2n\beta\sum_{i,j=1}\|\boldsymbol{r}_i-\boldsymbol{r}_j\|^2 \\
&\le -nk_eV_1^{\frac{\alpha_1+1}{2\alpha_1}} + 2n\beta V_1^{\frac{1}{2}}
\end{aligned} \tag{13}
$$

If we let

$$
-nk_eV_1^{\frac{\alpha_1+1}{2\alpha_1}} + 2n\beta V_1^{\frac{1}{2}} \le -\eta V_1^{\frac{1}{2}}
$$

i.e.

$$
\begin{aligned}
-nk_eV_1^{\frac{1}{2\alpha_1}} + 2n\beta &\le -\eta \\
V_1 &\ge \left(\frac{\eta+2n\beta}{nk_e}\right)^{2\alpha_1} := \epsilon^2
\end{aligned}
$$

where $\eta > 0$ is a positive constant and $f(\beta, k_e, \alpha_1)$ is a single-valued function to the inputs, then

$$
\dot{V}_1 \le -\eta V_1^{\frac{1}{2}}
$$

which means the Lyapunov function will converge to the set $[0, f(\beta, k_e, \alpha_1)]$ in finite time

$$
T_1 \le 2\frac{V_1^{\frac{1}{2}}(0)-\epsilon}{\eta}
$$

and will stay within the set, i.e. $V_1(t) \in [0, f(\beta, k_e, \alpha_1)], \forall t > T_1$.

Since $V_1 = \sum_{i,j=1}(\boldsymbol{r}_i-\boldsymbol{r}_j)^2$, for any two followers i, j, the difference between their estimates has

$$
\|\boldsymbol{r}_i-\boldsymbol{r}_j\| \le \sqrt{V_1}
$$

before the settling time T_1. In addition,

$$
\sum_{i=1}^{n}\boldsymbol{r}_i(t) = k_e\int_0^t\sum_{i=1}^{n}\sum_{j\in\boldsymbol{N}_i} a_{ij}(\boldsymbol{r}_j-\boldsymbol{r}_i)^{\frac{1}{\alpha_1}} + \sum_{i=1}^{n}\tilde{\boldsymbol{p}}_i
$$

Since

$$
\sum_{i=1}^{n}\sum_{j\in\boldsymbol{N}_i} a_{ij}(\boldsymbol{r}_j-\boldsymbol{r}_i)^{\frac{1}{\alpha_1}} = 0
$$

and

$$
\sum_{i=1}^{n}\tilde{\boldsymbol{p}}_i = \sum_{i=1}^{n}\frac{n}{m}\sum_{j\in\boldsymbol{N}_i^T}\frac{1}{|\boldsymbol{N}_j^F|}\boldsymbol{p}_j^t = \frac{n}{m}\sum_{i=1}^{m}\boldsymbol{p}_j^t = n\bar{\boldsymbol{p}}^t
$$

Therefore,

$$
\frac{1}{n}\sum_{i=1}^{n}\boldsymbol{r}_i = \bar{\boldsymbol{p}}_t
$$

For any follower $i \in \mathscr{V}_F$, the error between the real LAP and the output of the estimate in (7) is

$$\begin{aligned}\|\boldsymbol{r}_i - \bar{\boldsymbol{p}}^t\| &= \|\boldsymbol{r}_i - \frac{1}{n}\sum_{j=1}^{n}\boldsymbol{r}_j\| = \|\frac{1}{n}\sum_{j=1}^{n}(\boldsymbol{r}_i - \boldsymbol{r}_j)\| \\ &\le \frac{1}{n}\sum_{j=1}^{n}\|(\boldsymbol{r}_i - \boldsymbol{r}_j)\| \le \epsilon\end{aligned}$$

In conclusion, we present the following theorem:

Theorem 2. *Given Assumption 1–3, considering the system in (1) and (2), if each follower in the MRS maintains an estimator (7), there exists a settling time T_1 and a positive threshold ϵ, such that,*

$$\lim_{t > T_1} \|\boldsymbol{r}_i - \bar{\boldsymbol{p}}^t\| \le \epsilon \tag{14}$$

where the threshold can be adjusted by tuning the parameters in the estimator.

Proof. The proof has been derived above and thus omitted. □

Remark 3. Theorem 2 ensures that the proposed continuous estimator can converge to an adjustable accuracy in finite time. The main advantage is the continuity of the outputs $\boldsymbol{r}$ and $\dot{\boldsymbol{r}}$. As done by prevailing methods in [22–24], these estimates are directly fed into the enclosing controller. As a result, the proposed estimator in (7) can avoid the chattering phenomenon in the control commands. In addition, The upper bound of estimating accuracy can be adjusted by tuning the parameters k_e, α_1 in the estimator. In practice, the preferred principles for determining k_e and α_1 given the desired accuracy ϵ_d and settling time $T_{1,d}$ could be:

1. choose a large $k_e > 0$ such that $nk_e > \eta + 2n\beta$.
2. α_1 should satisfy:

$$\alpha_1 > \frac{\ln \epsilon_d}{\ln(\eta + 2n\beta) - \ln(nk_e)}$$

and

$$\alpha_1 > \frac{\ln\left[V_1^{\frac{1}{2}}(0) - \frac{T_{1,d}\, n(k_e - 2\beta)}{2}\right]}{\ln(\eta + 2n\beta) - \ln(nk_e)}$$

Remark 4. As shown in Fig. 4(C), the consensus error with fractional-order term can continuously slide toward the origin as it diminishes in magnitude. In favor of such property, the consensus error can remain stable and smoothing within a small neighborhood around zero, which helps prevent the alternatively rising and falling of the error between any two neighboring agents when compared with the unit-vector-based estimator. Therefore, the derivatives of their internal state $\boldsymbol{\Phi}_i$ would not intermittently jump around, and thus the derivatives of $\boldsymbol{r}_i$ can be stable and smooth.

4.2. The second-order continuous estimator

The previous estimator is easily implemented in practice with bounded accuracy in theory. As a complement, this subsection proposes a second-order continuous estimator as follows:

$$\begin{cases}\dot{\boldsymbol{q}}_i = \boldsymbol{\xi}_i & \text{(a)}\\ \dot{\boldsymbol{\xi}}_i = -\tau_i \frac{\boldsymbol{\Phi}_i}{\|\boldsymbol{\Phi}_i\|} - \zeta_i \sum_{i\in\mathscr{V}_F} a_{ij}(\boldsymbol{\Phi}_i - \boldsymbol{\Phi}_j)^{\mu} & \text{(b)}\\ \boldsymbol{\Phi}_i = \alpha_2 \sum_{i\in\mathscr{V}_F} a_{ij}(\boldsymbol{r}_i - \boldsymbol{r}_j) + \alpha_3 \sum_{i\in\mathscr{V}_F} a_{ij}(\boldsymbol{s}_i - \boldsymbol{s}_j) & \text{(c)}\\ \boldsymbol{r}_i = \boldsymbol{q}_i + \tilde{\boldsymbol{p}}_i & \text{(d)}\\ \boldsymbol{s}_i = \boldsymbol{\xi}_i + \tilde{\boldsymbol{v}}_i & \text{(e)}\\ \tilde{\boldsymbol{p}}_i = \frac{n}{m}\sum_{j\in \boldsymbol{N}_i^T} \frac{1}{|\boldsymbol{N}_j^F|}\boldsymbol{p}_j^t & \text{(f)}\\ \tilde{\boldsymbol{v}}_i = \frac{n}{m}\sum_{j\in \boldsymbol{N}_i^T} \frac{1}{|\boldsymbol{N}_j^F|}\boldsymbol{v}_j^t & \text{(g)}\end{cases} \tag{15}$$

where $\boldsymbol{q}_i, \boldsymbol{\xi}_i$ and $\boldsymbol{\Phi}_i$ are the internal states with the requirements $\sum_{i=1}^{n} \boldsymbol{q}_i(0) = 0$ and $\sum_{i=1}^{n} \boldsymbol{\xi}_i(0) = 0$. $\boldsymbol{r}_i$ and $\boldsymbol{s}_i$ are the estimates of the position and velocity of the GCT at ith agents. $\zeta_i > 0, \forall i \in \mathscr{V}_F$ are positive constants, $\mu > 2$ is an odd integer. $\tau_i, \zeta_i, \alpha_2, \alpha_3$ are the positive parameters to be determined. Note that such an estimator requires that the follower can both measure the position and velocity of the observed targets. Its flowchart is shown in Fig. 5.

For the simplicity of the following derivations, let us introduce the vectorized notations. We implement the bold unsubscripted notation $\boldsymbol{\Delta}$ as the vectorization of $\boldsymbol{\Delta}_i, \forall i \in \mathscr{V}_F$ or $\forall i \in \mathscr{V}_L$, here $\boldsymbol{\Delta}$ can be any letter used in this paper. For example, we denote

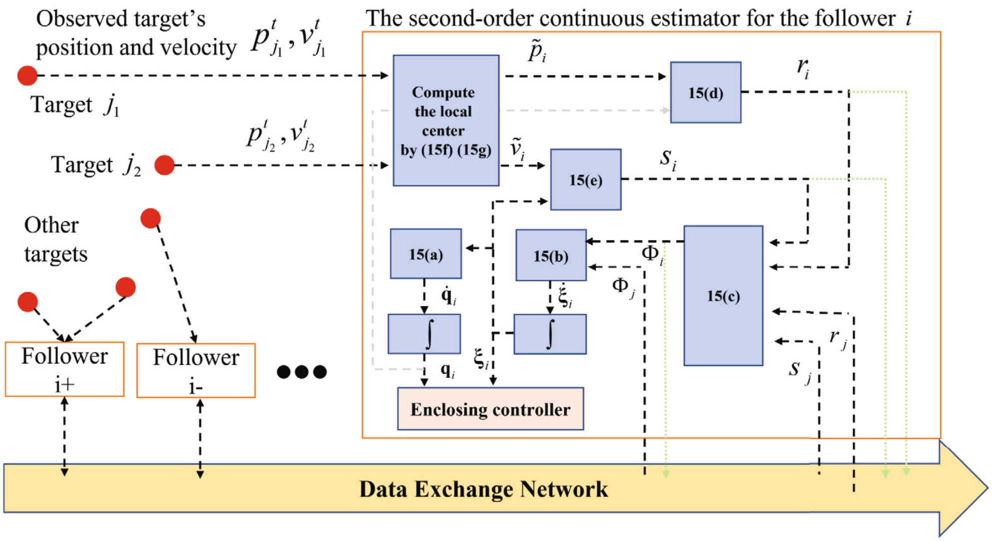

Fig. 5. The flowchart of the second-order continuous estimator. It takes as input the observation of targets' positions and velocities, the estimated position and velocity of the GCT from other robots, and the exchanged internal states $\boldsymbol{\Phi}_i$.

$\boldsymbol{r} = [\boldsymbol{r}_1^T, \boldsymbol{r}_2^T, \ldots, \boldsymbol{r}_n^T]^T$ and $\boldsymbol{s} = [\boldsymbol{s}_1^T, \boldsymbol{s}_2^T, \ldots, \boldsymbol{s}_n^T]^T$ the vectors containing the estimates of all followers. In addition, let us define the average consensus errors as follows:

$$\tilde{\boldsymbol{r}}_i = \boldsymbol{r}_i - \frac{1}{n}\sum_{j\in\mathcal{V}_F} \boldsymbol{r}_j$$

and

$$\tilde{\boldsymbol{s}}_i = \boldsymbol{s}_i - \frac{1}{n}\sum_{j\in\mathcal{V}_F} \boldsymbol{s}_j$$

Therefore, the vectorized expression can be derived by

$$\tilde{\boldsymbol{r}} = \boldsymbol{M}\boldsymbol{r}$$
$$\tilde{\boldsymbol{s}} = \boldsymbol{M}\boldsymbol{s}$$

where $\boldsymbol{M} \in \mathbb{R}^{2n\times 2n} = (\boldsymbol{I}_n - \frac{1}{n}\mathbf{1}_n) \otimes \boldsymbol{I}_2$ with $\boldsymbol{I}_n \in \mathbb{R}^{n\times n}$ the identity matrix and $\mathbf{1}_n \in \mathbb{R}^{n\times n}$ the square matrix whose elements are all one. Thereby, their derivatives can be achieved:

$$\dot{\tilde{\boldsymbol{r}}} = \tilde{\boldsymbol{s}}$$
$$\dot{\tilde{\boldsymbol{s}}} = \boldsymbol{M}\left(\dot{\boldsymbol{\xi}} + \dot{\tilde{\boldsymbol{v}}}\right)$$

Let $\boldsymbol{y}_i = \sum_{i\in\mathcal{V}_F} a_{ij}(\boldsymbol{r}_i - \boldsymbol{r}_j)$ and $\boldsymbol{z}_i = \sum_{i\in\mathcal{V}_F} a_{ij}(\boldsymbol{s}_i - \boldsymbol{s}_j)$, we can derive the following equations by the property of the Laplacian matrix $\boldsymbol{L}$:

$$(\boldsymbol{L}\otimes\boldsymbol{I}_2)\tilde{\boldsymbol{r}} = (\boldsymbol{L}\otimes\boldsymbol{I}_2)\boldsymbol{M}\boldsymbol{r} = (\boldsymbol{L}\otimes\boldsymbol{I}_2)\boldsymbol{r} = \boldsymbol{y}$$
$$(\boldsymbol{L}\otimes\boldsymbol{I}_2)\tilde{\boldsymbol{s}} = (\boldsymbol{L}\otimes\boldsymbol{I}_2)\boldsymbol{M}\boldsymbol{s} = (\boldsymbol{L}\otimes\boldsymbol{I}_2)\boldsymbol{s} = \boldsymbol{z}$$

Choosing the candidate Lyapunov function as:

$$V(t) = \tilde{\boldsymbol{r}}^T\left(\alpha_2\alpha_3\boldsymbol{L}^2\otimes\boldsymbol{I}_2\right)\tilde{\boldsymbol{r}} + \tilde{\boldsymbol{r}}^T\left(\alpha_2\boldsymbol{L}\otimes\boldsymbol{I}_2\right)\tilde{\boldsymbol{s}} + \frac{1}{2}\tilde{\boldsymbol{s}}^T\left(\alpha_3\boldsymbol{L}\otimes\boldsymbol{I}_2\right)\tilde{\boldsymbol{s}} \tag{16}$$

We first show that this function is semi-definite positive under some mild conditions by showing that

$$\boldsymbol{P} = \begin{bmatrix} \alpha_2\alpha_3\boldsymbol{L}^2 & \frac{\alpha_2}{2}\boldsymbol{L} \\ \frac{\alpha_2}{2}\boldsymbol{L} & \frac{\alpha_3}{2}\boldsymbol{L}\end{bmatrix} \otimes \boldsymbol{I}_2 \geq 0$$

Consequentially, if $\lambda_2 > \frac{\alpha_2}{4\alpha_3}$, the candidate Lyapunov function is guaranteed semi-definite positive.

Taking the derivative of (16) yields:

$$\begin{aligned}\dot{V} &= 2\alpha_2\alpha_3\tilde{\boldsymbol{r}}^T(\boldsymbol{L}^2\otimes\boldsymbol{I}_2)\tilde{\boldsymbol{s}} + \alpha_2\tilde{\boldsymbol{s}}^T(\boldsymbol{L}\otimes\boldsymbol{I}_2)\tilde{\boldsymbol{s}} \\ &+ \underbrace{(\alpha_2\tilde{\boldsymbol{r}}^T + \alpha_3\tilde{\boldsymbol{s}}^T)(\boldsymbol{L}\otimes\boldsymbol{I}_2)\dot{\tilde{\boldsymbol{s}}}}_{A}\end{aligned} \tag{17}$$

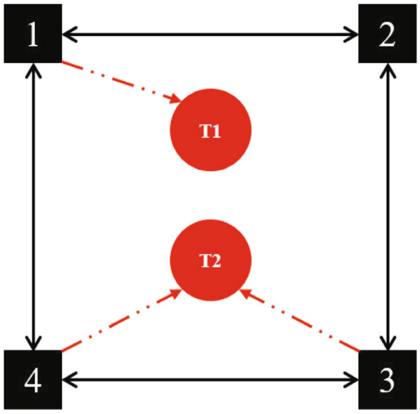

Fig. 6. The observation and communication topology of the MTECP in the simulation, where the red circles and black rectangles are the targets and followers respectively. The solid black double-ended arrows are the communication network among followers, while the dashed red single-ended arrows are the observation links between the followers and targets.

Recalling that $\boldsymbol{\Phi} = \alpha_2 \boldsymbol{y} + \alpha_3 \boldsymbol{z}$, then term A in (17) can be written as:

$$\begin{aligned} \text{term A} &= (\alpha_2 \tilde{\boldsymbol{r}}^T + \alpha_3 \tilde{\boldsymbol{s}}^T)(\boldsymbol{L} \otimes \boldsymbol{I}_2)\boldsymbol{M}\left(\dot{\boldsymbol{\xi}} + \dot{\boldsymbol{v}}\right) \\ &= (\alpha_2 \tilde{\boldsymbol{r}}^T + \alpha_3 \tilde{\boldsymbol{s}}^T)(\boldsymbol{L} \otimes \boldsymbol{I}_2)\left(\dot{\boldsymbol{\xi}} + \dot{\boldsymbol{v}}\right) \\ &= \boldsymbol{\Phi}^T\left(\dot{\boldsymbol{\xi}} + \dot{\boldsymbol{v}}\right) \\ &= -\sum_{i=1}^{n} \zeta_i \boldsymbol{\Phi}_i^T \sum_{j \in \mathcal{V}_F} a_{ij}(\boldsymbol{\Phi}_i - \boldsymbol{\Phi}_j)^{\mu} - \sum_{i=1}^{n} \tau_i \frac{\boldsymbol{\Phi}_i^T \boldsymbol{\Phi}_i}{\|\boldsymbol{\Phi}_i\|} + \boldsymbol{\Phi}^T \dot{\boldsymbol{v}} \end{aligned} \tag{18}$$

Easily, we can get

$$\boldsymbol{\Phi}^T \boldsymbol{\Phi} = \alpha_2^2 \boldsymbol{y}^T \boldsymbol{y} + 2\alpha_2 \alpha_3 \boldsymbol{y}^T \boldsymbol{z} + \alpha_3^2 \boldsymbol{z}^T \boldsymbol{z} \tag{19}$$

Substituting (18) and (19) into (17) yields

$$\begin{aligned} \dot{V} \leq & -\alpha_2^2 \boldsymbol{y}^T \boldsymbol{y} - (\alpha_3^2 - \frac{\alpha_2}{\lambda_2})\boldsymbol{z}^T \boldsymbol{z} - \frac{\min(\zeta_i)}{2} \sum_{i=1}^{n} \sum_{j \in \mathcal{V}_F} a_{ij} \|\boldsymbol{\Phi}_i - \boldsymbol{\Phi}_j\|^{\mu+1} \\ & - \left(\min(\tau_i) - \max(\|\boldsymbol{a}_j^t\|)\right) \sum_{i=1}^{n} \|\boldsymbol{\Phi}_i\| \leq 0 \end{aligned} \tag{20}$$

If $(\min(\tau_i) - \gamma > 0)$, the equality holds only when $\boldsymbol{y}$ and $\boldsymbol{z}$ reach to zeros, which implies that the average consensus errors $\tilde{\boldsymbol{r}}$ and $\tilde{\boldsymbol{s}}$ are all zeros. Therefore, we can conclude by the Barbalat's lemma that $(\tilde{\boldsymbol{r}}, \tilde{\boldsymbol{s}})$ can converge to zeros asymptotically.

In the following, we show that the convergence can also be achieved in finite-time. It can be concluded accordingly that $\tilde{\boldsymbol{r}} \neq \boldsymbol{0}, \tilde{\boldsymbol{s}} \neq \boldsymbol{0}$ and $\boldsymbol{\Phi}^T \boldsymbol{\Phi} > 0$ until the consensus is reached. Let us further define $\boldsymbol{\epsilon}_i = [\alpha_2 \boldsymbol{y}_i^T, \alpha_3 \boldsymbol{z}_i^T]$ and $\tilde{\boldsymbol{\epsilon}}_i = [\tilde{\boldsymbol{r}}_i^T, \tilde{\boldsymbol{s}}_i^T]^T$, then we can derive:

$$\boldsymbol{\Phi}^T \boldsymbol{\Phi} \geq k_{\varphi} \boldsymbol{\epsilon}^T \boldsymbol{\epsilon} \geq k_{\varphi} \lambda_2 \min(\alpha_2^2, \alpha_3^2) \tilde{\boldsymbol{\epsilon}}^T \tilde{\boldsymbol{\epsilon}} \tag{21}$$

where $k_{\varphi} = \min_{\frac{\epsilon}{\|\epsilon\|}} \left[\left(\frac{\epsilon}{\|\epsilon\|}\right)^T \begin{bmatrix} 1, 1 \\ 1, 1 \end{bmatrix} \otimes \boldsymbol{I}_2 \left(\frac{\epsilon}{\|\epsilon\|}\right) \right] > 0$ according to the Lemma 6 in [32]. Then from the definition of the Lyapunov function (16), we know that

$$V = \tilde{\boldsymbol{\epsilon}}^T \boldsymbol{P} \tilde{\boldsymbol{\epsilon}} \leq \lambda_{max}(\boldsymbol{P}) \tilde{\boldsymbol{\epsilon}}^T \tilde{\boldsymbol{\epsilon}} \tag{22}$$

Substituting (21) and (22) back into (20) derives:

$$\dot{V} \leq -k_v V^{\frac{1}{2}}$$

where $k_v = \left(\min(\tau_i) - \max(\|\dot{\boldsymbol{v}}_i\|)\right) \sqrt{\frac{k_{\varphi} \lambda_2}{\lambda_{max}(\boldsymbol{P})}} \min(\alpha_2, \alpha_3)$. Therefore, we can conclude from Theorem 1 that $(\tilde{\boldsymbol{r}}, \tilde{\boldsymbol{s}})$ is also finite-time convergent with the settling time $T_2 \leq \frac{2V^{\frac{1}{2}}(0)}{k_v}$, implying that $\lim_{t > T_2} |\boldsymbol{r}_i - \boldsymbol{r}_j| = 0$ and $\lim_{t > T_2} |\boldsymbol{s}_i - \boldsymbol{s}_j| = 0$.

In the presence of the initial conditions of the internal states $\sum_{i=1}^{n} \boldsymbol{q}_i(0) = \boldsymbol{0}$ and $\sum_{i=1}^{n} \boldsymbol{\xi}_i(0) = \boldsymbol{0}$, we can derive that

$$\sum_{i=1}^{n} \boldsymbol{q}_i(t) = -\int_0^t \int_0^t \sum_{i=1}^{n} \left[\tau_i \frac{\boldsymbol{\Phi}_i}{|\boldsymbol{\Phi}_i|} + \zeta_i \sum_{i \in \mathcal{V}_F} a_{ij}(\boldsymbol{\Phi}_i - \boldsymbol{\Phi}_j)^{\mu} \right] dt^2 = \boldsymbol{0}$$

Table 1
Initial positions for the simulation case.

Nodes	Followers				Targets	
	F_1	F_1	F_1	F_1	L_1	L_2
Pos(m)	[10; −20]	[18; 12]	[4; 12]	[−2; 16]	[0; 0]	[1; 1]

Table 2
Parameters of the estimators.

Estimators	(5)	(7)		(15)			
Parameters	k_{sgn}	k_e	α_1	α_2	α_3	τ_i	ζ
Values	3	3	$\frac{3}{7}$	1	5	5	10

Therefore, we can have

$$\sum_{i=1}^{n} \boldsymbol{r}_i = \sum_{i=1}^{n} \tilde{\boldsymbol{p}}_i = n\bar{\boldsymbol{p}}^t$$
$$\sum_{i=1}^{n} \boldsymbol{s}_i = \sum_{i=1}^{n} \tilde{\boldsymbol{v}}_i = n\bar{\boldsymbol{v}}^t$$

Therefore, the estimator in (15) can precisely track the position and velocity of the GCT in finite time. We conclude these results with the following theorem,

Theorem 3. *Given Assumption 1–3 and considering the MTECP consisting of (1) and (2), the estimator in (15) can exactly track the GCT and its velocity in finite time i.e.*

$$\lim_{t>T_2} |\boldsymbol{r}_i - \bar{\boldsymbol{p}}^t| = 0$$
$$\lim_{t>T_2} |\boldsymbol{s}_i - \bar{\boldsymbol{v}}^t| = 0$$

if $4\lambda_2\alpha_3 - \alpha_2 > 0$ *and* $\min(\tau_i) - \gamma > 0$.

Proof. The proof can be immediately derived from the above analysis. It is thus omitted. □

Remark 5. The continuity of the estimator in (15) comes from the integration of the internal states ξ_i and its derivative $\dot{\xi}_i$. Since the estimated position and velocity of the GCT are feedback into the enclosing controller, the discontinuity of this estimator only appears in the acceleration phase and therefore can avoid chattering phenomenon in the control commands of followers. Note that the inclusion of the unit-vector term $\frac{\boldsymbol{\Phi}_i}{|\boldsymbol{\Phi}_i|}$ is crucial for achieving precise estimation of the GCT when compared with the fractional-order estimator in (7). By integrating the unit-vector term over time, the estimator averages out any sudden changes or discontinuities in the unit-vector term, which therefore can enhance the overall performance and reliability of the final enclosing controller, leading to a more stable and predictable output.

Remark 6. As shown from the theoretical analysis, both estimators can avoid the chattering phenomenon in the enclosing control problem. The fractional-order estimator is comparatively easily implemented with less input data. To realize the second-order estimator, not only do the followers need to observe the position and velocity for the necessary targets to satisfy Assumption 2, but the followers also need to exchange with neighbors their estimates $\boldsymbol{r}_i, \boldsymbol{s}_i$, and the internal state $\boldsymbol{\Phi}_i$ by the communication network. It is therefore more complex compared with the fractional-order estimator. However, the second-order estimator can exactly track the real GCT in theory i.e. with no estimation error, while the fractional-order estimator suffers from a bounded precision.

Remark 7. Though the second-order estimator in (15) seems more complex than the fractional-order one, the selection of the four parameters $\alpha_2, \alpha_3, \tau_i$ and ζ is quite easier in practice. In the presence of the prior knowledge of the communication topology and the upper bound of targets' acceleration, we can first fix a positive value to α_2 and then choose a proper α_3 such that $\alpha_3 > \frac{\alpha_2}{4\lambda_2}$. Besides, τ_i can be determined by uniformly choosing a constant value that is bigger than the upper bound of targets' acceleration γ.

5. Simulation

This section presents the comparison of performance of the proposed estimators in (7) (15) and the discontinuous one in (5), which are tested under the scenario of MTECP with four followers and two moving targets in 2-D plane. The observation and communication network is indicated in Fig. 6. Their initial positions are deployed according to Table 1. The equations of time-varying targets are:

$$\boldsymbol{v}_1^t = \begin{bmatrix} 1 \\ 0 \end{bmatrix} \quad \boldsymbol{v}_2^t = \begin{bmatrix} 1 \\ \frac{1}{2}\cos(\frac{t}{10} + \frac{\pi}{3}) \end{bmatrix}$$

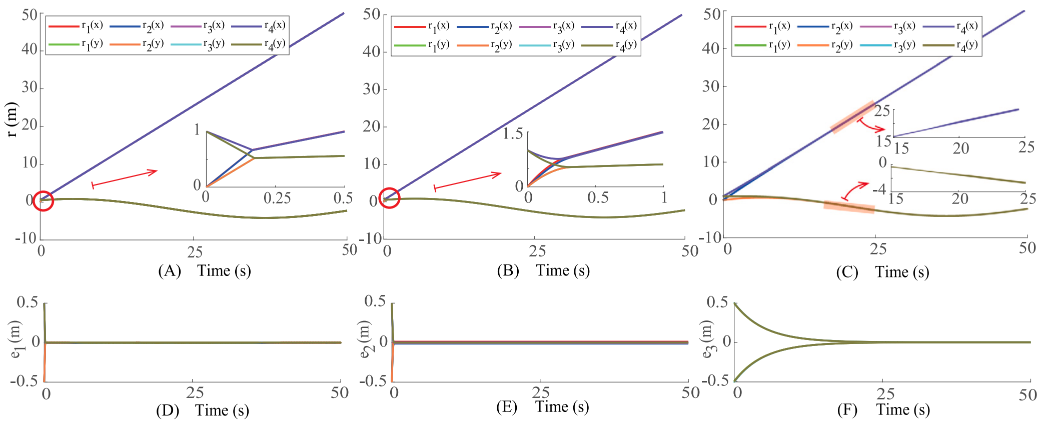

Fig. 7. The output $\boldsymbol{r}_i$ of three estimators and the errors between the real GCT and the estimated r_i for all four followers. Fig {A, D}: discontinuous estimator (5), Fig {B, E}: the fractional-order estimator (7) and {C, F}: the second-order estimator (15).

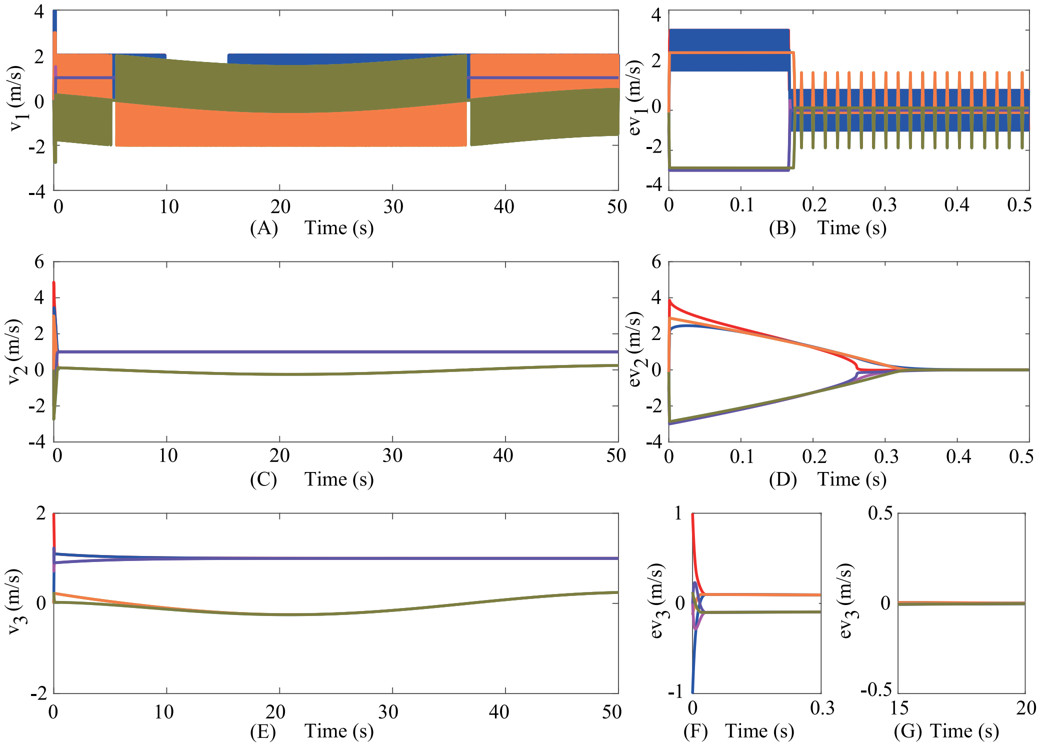

Fig. 8. The estimated velocity $\dot{\boldsymbol{r}}_i$ of three estimators, and the their errors compared with the real velocity of the GCT. Fig {A, B}: discontinuous estimator (5), Fig {C, D}: the fractional-order estimator (7) and {E, F, G}: the second-order estimator (15).

Therefore, the upper bound of target velocities and accelerations are $\beta = \frac{\sqrt{5}}{2}, \gamma = 0.05$. The parameters of the three estimators are given in Table 2.

The simulation results are demonstrated in Figs. 7 and 8 where the performance of tracking the position and velocity of the real GCT for all four followers.

Fig. 7 shows that all three tested estimators can precisely track the real GCT. Compared with the benchmark (5) as shown in Fig. 7(A, D), the convergence of the fractional-order estimator becomes non-linear in Fig. 7(B) with similar settling time. Though theoretical analysis only guarantees bounded tracking error, simulation results in Fig. 7(E) demonstrate comparable precision of the fractional-order estimator. Regarding the second-order estimator in (15), it becomes much slower to converge to the real GCT, spending about 20 s as compared to ≈0.2 s in benchmark and ≈0.3 s in the fraction-order estimator.

Fig. 8(A, C, E) present the estimated velocity of the GCT, demonstrated by the derivative of output i.e. $v_1, v_2 \to \dot{\boldsymbol{r}}_i$ for the first-order estimators (5), (7), and $v_3 \to \boldsymbol{s}_i$ for the second-order estimator (15). The focused chattering phenomenon is exposed in

Fig. 8(A, B), where we can see all four followers exhibit undesirable oscillations starting around 0.2s when the estimator starts getting convergent. In comparison, the proposed two continuous estimators successfully remove such impact in Fig. 8(C,E). Fig. 8(B, D, F, G) are the differences between the estimated velocities from these estimators, and the real values. Fig. 8(D) details the evolution of the estimated errors under the proposed fractional-order estimator for all four followers before convergence, showing the continuity and steady of the tracking effect. Fig. 8(F) shows that the consensus errors of e_{vx} and e_{vy} independently converge at the initial stage. Then they are stabilized to the origin in finite time at around 15 s as shown in Fig. 8(G).

6. Conclusion

The chattering problem of distributively estimating the time-varying position and velocity of the GCT under the scenario of MTECP is considered in this work. The occurrence of chattering can detrimentally affect robotic systems, leading to a loss of control precision, heightened wear of robotic components, and increased power consumption. In response, this work introduces two continuous estimators to mitigate chattering during the estimation phase, deviating from SOTA approaches that directly feed forward the estimated position and velocity of the GCT to the enclosing controller. Both theoretical analysis and simulation results demonstrate that the proposed estimator can precisely and continuously track the real GCT in finite time.

Some open problems may be considered in the future. For example, how to relax the assumptions to meet realistic constraints, how to enclosing multiple targets in the three-dimension space, and so on. Future endeavors may also focus on exploring more realistic sensing methods (e.g. time-varying topology of both communication and observation), extending the investigation to encompass more complex robot dynamics, and conducting physical experiments to evaluate the potential application on real robotic swarms.

CRediT authorship contribution statement

Liang Zhang: Writing – review & editing, Writing – original draft, Visualization, Validation, Software, Resources, Project administration, Methodology, Investigation, Funding acquisition, Formal analysis, Data curation, Conceptualization. **Jun Song:** Validation, Software, Resources, Methodology, Data curation, Conceptualization. **Shuping He:** Writing – review & editing, Writing – original draft, Supervision, Project administration, Funding acquisition, Conceptualization.

Declaration of competing interest

The authors declare that they have no conflicts of interest to this work. We still declare that we do not have any commercial or associative interest that represents a conflict of interest in connection with the work submitted.

Acknowledgments

This work was supported in part by the National Natural Science Foundation of China (No. 62303002 and No. 62073001), the University Synergy Innovation Program of Anhui Province, China (No. GXXT-2021-010), the Key Support Program of University Outstanding Youth Talent of Anhui Province, China (No. gxydZD2017001) and the Anhui Education Department Research Project, China (KJ2020A0029).

References

[1] F. Berlinger, M. Gauci, R. Nagpal, Implicit coordination for 3D underwater collective behaviors in a fish-inspired robot swarm, Science Robotics 6 (50) (2021).
[2] M. Dorigo, G. Theraulaz, V. Trianni, Reflections on the future of swarm robotics, Science Robotics 5 (49) (2020).
[3] Y. Lan, G. Yan, Z. Lin, Distributed control of cooperative target enclosing based on reachability and invariance analysis, Systems Control Lett. 59 (7) (2010) 381–389.
[4] R. Zheng, Y. Liu, D. Sun, Enclosing a target by nonholonomic mobile robots with bearing-only measurements, Automatica 53 (2015) 400–407.
[5] C. Li, L. Chen, Y. Guo, Y. Lyu, Cooperative surrounding control with collision avoidance for networked Lagrangian systems, J. Franklin Inst. 355 (12) (2018) 5182–5202.
[6] T.-H. Kim, T. Sugie, Cooperative control for target-capturing task based on a cyclic pursuit strategy, Automatica 43 (8) (2007) 1426–1431.
[7] S. Hara, T.-H. Kim, Y. Hori, Distributed formation control for target-enclosing operations based on a cyclic pursuit strategy, IFAC Proc. Vol. 41 (2) (2008) 6602–6607.
[8] J. Guo, G. Yan, Z. Lin, Local control strategy for moving-target-enclosing under dynamically changing network topology, Systems Control Lett. 59 (10) (2010) 654–661.
[9] K. Lu, S.-L. Dai, X. Jin, Cooperative constrained enclosing control of multirobot systems in obstacle environments, IEEE Trans. Control Netw. Syst. (2023) 1–12, http://dx.doi.org/10.1109/TCNS.2023.3299151.
[10] K. Lu, S.-L. Dai, X. Jin, Adaptive angle-constrained enclosing control for multirobot systems using bearing measurements, IEEE Trans. Autom. Control 69 (2) (2024) 1324–1331, http://dx.doi.org/10.1109/TAC.2023.3303096.
[11] X. Shao, F. Zhang, W. Zhang, J. Na, Finite-time composite learning-based elliptical enclosing control for nonholonomic robots under a GPS-denied environment, IEEE Trans. Syst. Man Cybern. A 53 (9) (2023) 5282–5294, http://dx.doi.org/10.1109/TSMC.2022.3215474.
[12] B. Xu, H.-T. Zhang, H. Meng, B. Hu, D. Chen, G. Chen, Moving target surrounding control of linear multiagent systems with input saturation, IEEE Trans. Syst. Man Cybern. A 52 (3) (2022) 1705–1715, http://dx.doi.org/10.1109/TSMC.2020.3030706.
[13] S. Ju, J. Wang, L. Dou, MPC-based cooperative enclosing for nonholonomic mobile agents under input constraint and unknown disturbance, IEEE Trans. Cybern. 53 (2) (2022) 845–858.

[14] X. Peng, K. Guo, X. Li, Z. Geng, Cooperative moving-target enclosing control for multiple nonholonomic vehicles using feedback linearization approach, IEEE Trans. Syst. Man Cybern. A 51 (8) (2021) 4929–4935, http://dx.doi.org/10.1109/TSMC.2019.2944539.

[15] L. Dou, X. Yu, L. Liu, X. Wang, G. Feng, Moving-target enclosing control for mobile agents with collision avoidance, IEEE Trans. Control Netw. Syst. 8 (4) (2021) 1669–1679.

[16] Z. Peng, Y. Jiang, J. Wang, Event-triggered dynamic surface control of an underactuated autonomous surface vehicle for target enclosing, IEEE Trans. Ind. Electron. 68 (4) (2021) 3402–3412, http://dx.doi.org/10.1109/TIE.2020.2978713.

[17] X. Liu, K. Liu, T. Hu, Q. Zhang, Formation control for moving target enclosing via relative localization, in: 2023 62nd IEEE Conference on Decision and Control, CDC, IEEE, 2023, pp. 1400–1405.

[18] F. Chen, W. Ren, Y. Cao, Surrounding control in cooperative agent networks, Systems Control Lett. 59 (11) (2010) 704–712.

[19] L. Zhang, Z. Zhang, Y. Qiao, X. Wei, Surrounding control in cooperative second-order agent networks, in: IECON 2017-43rd Annual Conference of the IEEE Industrial Electronics Society, IEEE, 2017, pp. 5604–5609.

[20] F. Chen, Y. Cao, W. Ren, Distributed average tracking of multiple time-varying reference signals with bounded derivatives, IEEE Trans. Autom. Control 57 (2012) 3169–3174.

[21] B. Xu, H.-T. Zhang, Y. Ding, W. Ren, Event-triggered surrounding formation control of multi-agent systems for multiple dynamic targets, IEEE Trans. Control Netw. Syst. (2022) http://dx.doi.org/10.1109/TCNS.2022.3210291, Early Access.

[22] B.B. Hu, H.T. Zhang, J. Wang, Multiple-target surrounding and collision avoidance with second-order nonlinear multiagent systems, IEEE Trans. Ind. Electron. 68 (2021) 7454–7463, http://dx.doi.org/10.1109/TIE.2020.3000092.

[23] Z.J. Ma, T. Kirubarajan, Y.Y. Li, Finite-time encirclement rotating tracking for surface formation targets with bearing-only measurements, Nonlinear Dynam. 105 (2021) 3323–3339, http://dx.doi.org/10.1007/s11071-021-06818-0.

[24] Y. Shi, R. Li, K.L. Teo, Cooperative enclosing control for multiple moving targets by a group of agents, Internat. J. Control 88 (1) (2015) 80–89.

[25] A. Sharghi, M. Baradarannia, F. Hashemzadeh, Finite-time-estimation-based surrounding control for a class of unknown nonlinear multi-agent systems, Nonlinear Dynam. 96 (3) (2019) 1795–1804.

[26] L. Zhang, Z. Li, P. Gao, Finite-time surrounding control of multi-agent systems with multiple targets, in: 2019 IEEE 8th Data Driven Control and Learning Systems Conference, DDCLS, IEEE, 2019, pp. 231–236.

[27] D. Ma, Y. Sun, Finite-time circle surrounding control for multi-agent systems, Int. J. Control Autom. Syst. 15 (4) (2017) 1536–1543.

[28] W. Keyue, L. Zhang, H. Shuping, Multiple-target enclosing control using bearing-only measurements, in: 2023 38th Youth Academic Annual Conference of Chinese Association of Automation, YAC, 2023, pp. 648–652, http://dx.doi.org/10.1109/YAC59482.2023.10401472.

[29] Target enclosing control for fixed-wing unmanned aerial vehicle in three dimensional space: An attractive vector approach, J. Franklin Inst. 361 (2) (2024) 1010–1022, http://dx.doi.org/10.1016/j.jfranklin.2023.12.041.

[30] L. Wang, F. Xiao, Finite-time consensus problems for networks of dynamic agents, IEEE Trans. Autom. Control 55 (4) (2010) 950–955.

[31] L. Zhang, Finite-time enclosing control for multiple moving targets: a continuous estimator approach, 2022, arXiv preprint arXiv:2202.00347.

[32] Y. Hu, Q. Lu, Y. Hu, Event-based communication and finite-time consensus control of mobile sensor networks for environmental monitoring, Sensors 18 (8) (2018) 2547.